

Mechanism of stochastic resonance enhancement in neuronal models driven by $1/f$ noise

Daichi Nozaki,^{1,2} James J. Collins,² and Yoshiharu Yamamoto³

¹*Motor Dysfunction Division, Research Institute of National Rehabilitation Center for the Disabled, 4-1 Namiki, Tokorozawa, Saitama 359-8555, Japan*

²*Center for BioDynamics and Department of Biomedical Engineering, Boston University, 44 Cummington Street, Boston, Massachusetts 02215*

³*Educational Physiology Laboratory, Graduate School of Education, The University of Tokyo, 7-3-1 Hongo, Bunkyo-ku, Tokyo 113-0033, Japan*

(Received 31 March 1999)

Noise can assist neurons in the detection of weak signals via a mechanism known as stochastic resonance (SR). In a previous study [Phys. Lett. A **243**, 281 (1998)], we showed that when colored noise with $1/f^\beta$ spectrum is added to the FitzHugh-Nagumo (FHN) neuronal model, the optimal noise variance for SR could be minimized with $\beta \approx 1$. In this study, we investigate analytically how the noise color (β) affects the SR profile in a linearized version of the FHN model. We demonstrate that the aforementioned effect of $1/f$ noise is related to the dynamical characteristics of the model neuron, i.e., the refractory period, the low-pass filtering effect of the membrane capacitance, and the high-pass filtering effect of the recovery variable.

[S1063-651X(99)11110-3]

PACS number(s): 87.80.Tq, 05.40.Ca

I. INTRODUCTION

It has recently been recognized that noise can enhance the response of nonlinear systems to weak signals, via a mechanism known as *stochastic resonance* (SR) [1]. SR was originally proposed to account for the periodic recurrences of the Earth's ice ages [2]. Thereafter, the phenomenon has been demonstrated in a wide range of systems, including bistable physical systems [1,3] and excitable systems [4,5]. The concept of SR has generated considerable interest in sensory biology, because it has been shown in several experimental studies that noise can assist neural systems in detecting subthreshold signals [4–6]. These results suggest a possible functional role for noise in sensory neurophysiological systems.

In the majority of previous SR studies, white noise with flat power spectrum (i.e., noise without any time correlation or with short-time correlation) has been used as the additive noise source. However, colored noise with a $1/f^\beta$ -type power spectrum (i.e., noise with long-range correlation) has been reported in many biological systems [7]. For instance, this type of noise has been found in the cat sensory system [8], the human autonomic nervous system [9], and the human motor system [10]. In most cases, the value of β is nearly equal to 1, which corresponds to well-known $1/f$ noise. (Note that for conventional white noise, $\beta=0$.)

In spite of the ubiquitousness of $1/f$ noise in biological and physiological systems, its functional significance, if any, has not been elucidated. Accordingly, it is interesting to consider whether $1/f^\beta$ noise can play a significant role for SR. A partial answer has already been provided: it has been shown that $1/f$ noise can induce SR in Schmitt triggers [11] and nondynamical threshold systems [12]. It is further interesting to consider whether $1/f$ noise can be better than conventional white noise for producing SR-type effects. Such an analysis may provide insight into the possible functional role of $1/f$ noise in biological and physiological systems.

Recently, we studied SR in a neuronal model driven by $1/f^\beta$ noise (with a relatively wide bandwidth) and examined how the value of β affects the SR profile [13]. We considered the FitzHugh-Nagumo (FHN) neuronal model [14]:

$$\varepsilon \dot{v} = v(v-a)(1-v) - w + A + S(t) + \xi(t), \quad (1)$$

$$\dot{w} = v - w - b, \quad (2)$$

where v is a fast variable representing the neuronal membrane voltage, w is a slow “recovery” variable, A is a constant (dc) input, $S(t)$ is an aperiodic subthreshold signal with zero mean, $\xi(t)$ is Gaussian $1/f^\beta$ noise ($0 \leq \beta \leq 2$) with zero mean and variance σ_N^2 [15], $\varepsilon \ll 1$, $a=0.5$, and $b=0.15$. SR effects were evaluated by examining the following input-output coherence measures [5]:

$$C_0 = \langle \langle S(t)R(t) \rangle \rangle, \quad (3)$$

$$C_1 = \frac{C_0}{\langle \langle S^2(t) \rangle \rangle^{1/2} \langle \langle [R(t) - \langle R(t) \rangle]^2 \rangle \rangle^{1/2}}, \quad (4)$$

where $R(t)$ is the firing frequency of the model neuron and the double angular brackets denote averages over time. C_0 and C_1 , respectively, represent the cross power and the normalized cross power between $S(t)$ and $R(t)$.

In Ref. [13], we showed computationally [16] that $1/f^\beta$ noise can induce SR, i.e., the above input-output coherence measures are maximized by a particular level (i.e., variance) of input noise. Furthermore, we found that the optimal noise variance that maximizes the coherence measures can be minimized with $\beta \approx 1$ (Fig. 1). This finding indicates that with $1/f$ noise, a weaker noise level, as compared with white noise, is sufficient for the model neuron to detect a given subthreshold signal. Our aims in this paper are (1) to extend this work by developing a mechanistic understanding of the

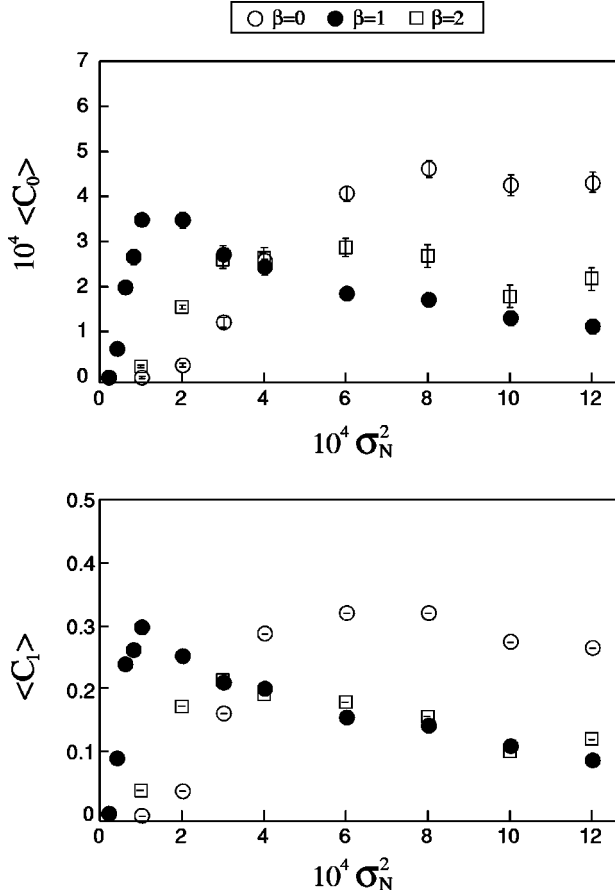


FIG. 1. Ensemble-averaged values and standard errors for C_0 and C_1 (500 trials) for different levels of input noise variance σ_N^2 in the FHN model (white noise, open circles; $1/f$ noise, filled circles; $1/f^2$ noise, open squares). The variance of $S(t)$ is 5.0×10^{-5} , $\varepsilon = 0.005$, and $A = 0.04$. The bandwidth of the noise is 0.0305–100 Hz.

effects of noise color (i.e., β) on SR profiles in model neurons, and (2) to investigate the effects of noise bandwidth on the SR profile. The latter aim is motivated by the fact that the statistical properties of $1/f^\beta$ noise depend on the data length; thus, it is natural to consider whether the observed effects of $1/f$ noise are robust to different noise bandwidths.

This paper is organized as follows. In Sec. II, we propose a linearized version of the FHN model and show that this system exhibits SR properties similar to those for the original FHN model, e.g., the optimal noise variance can be minimized with $\beta \approx 1$. We also introduce a method for obtaining the theoretical relationship between C_0 and σ_N^2 . In Sec. III, we show that in a neuronal model lacking a recovery variable, the optimal noise variance is minimized with $\beta = 2$. This finding indicates that a recovery variable is important for minimizing the optimal noise variance with $\beta \approx 1$. In Sec. IV we consider a resettable system with a refractory period, and using the method proposed in Sec. II, derive theoretical SR curves for the system. In Sec. V we investigate the influences of the refractory period and the effects of noise bandwidth on the SR profile. Finally, in Sec. VI, we summarize our results and discuss their implications.

II. LINEARIZED FHN MODEL WITHOUT RESET

When the value of ε in Eq. (1) is sufficiently small, the slow variable w [Eq. (2)] can be approximated as $w = v_* - b$, where the subscript $*$ indicates the fixed point. With this approximation and taking into account the nonlinear cubic term in Eq. (1), the FHN model can be regarded as having a fourth-order bistable potential function. For this case, the firing rate of the noise-driven FHN model corresponds to the escape rate of a particle over the potential barrier. In Ref. [5], Collins *et al.* considered a noise-driven FHN model with a subthreshold input signal and derived, using Kramers theory [17], a theoretical prediction for the input-output coherency as a function of the input noise intensity. In general, however, it is difficult to obtain the escape rate when the input noise has time correlations. (The input noise in Ref. [5] was white noise.) In Ref. [18], Hänggi *et al.* introduced a method for obtaining theoretical predictions of SR profiles when the input noise is exponentially correlated. This method, however, cannot be applied to $1/f^\beta$ noise because such noise cannot be expressed as an ordinary Markov process. To our knowledge, there is no general theoretical method for predicting the escape rate for systems with input noise with long-range correlation. Because of these limitations, we consider in this paper a simpler, linearized FHN (LFHN) model, which is described below.

When the neuronal firings are infrequent, the variables v and w primarily fluctuate around the stable fixed points (v_* and w_* , respectively). Thus, the cubic term in Eq. (1) can be expanded around the stable fixed point as $v_* - \gamma(v - v_*)$. In this study, we use $\gamma = 0.3$, which is nearly equal to $-\partial_v [v(v-a)(1-v)]|_{v=v_*}$. The dynamics around the resting values then obey the following equations:

$$\varepsilon \dot{v} = -\gamma v - w + S(t) + \xi(t), \quad (5)$$

$$\dot{w} = v - w, \quad (6)$$

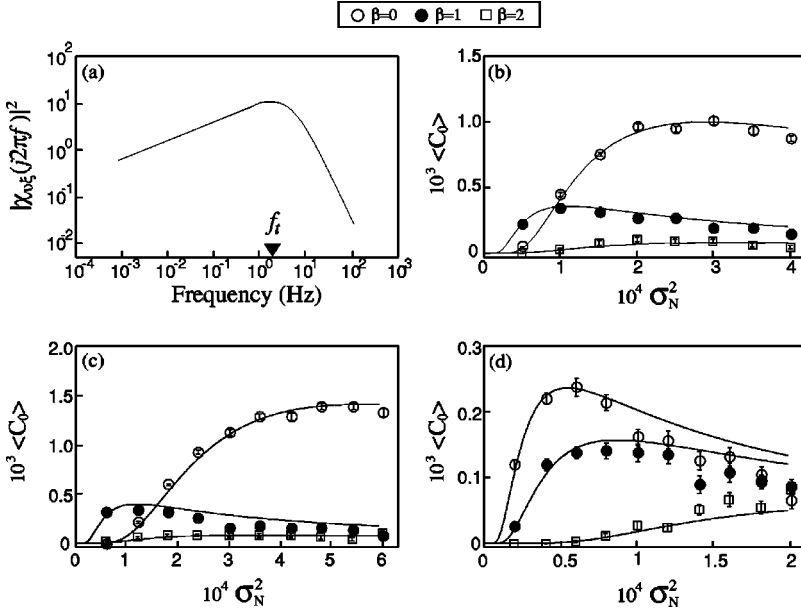
where we recast the variables as $v = v - v_*$ and $w = w - w_*$, for convenience. In the original FHN model, firing events can occur spontaneously when a sufficiently large input signal is added to the system. However, the LFHN model [Eqs. (5) and (6)] does not have a mechanism for generating action potentials. Thus, we assume that a narrow pulse is generated when the value of v crosses a threshold value with positive \dot{v} . In this section, we consider the case where the generation of pulses does not affect the values of v and w .

Because the dynamics of the LFHN model are linear, we can obtain the system's transfer function by applying the Laplace transform to Eqs. (5) and (6) for the case of $S(t) = 0$:

$$\varepsilon s V(s) = -\gamma V(s) - W(s) + N(s), \quad (7)$$

$$s W(s) = V(s) - W(s), \quad (8)$$

where $V(s)$, $W(s)$, and $N(s)$ are the Laplace transform of $v(t)$, $w(t)$, and $\xi(t)$, respectively. The transfer function from the input $\xi(t)$ to the output $v(t)$ is



$$\chi_{v\xi}(s) = \frac{V(s)}{N(s)} = \frac{1}{\varepsilon s + \gamma + 1/(s+1)}. \quad (9)$$

Therefore, the squared gain of the frequency response function is

$$|\chi_{v\xi}(j2\pi f)|^2 = \frac{(4\pi^2 f^2 + 1)^2}{[\gamma(4\pi^2 f^2 + 1) + 1]^2 + 4\pi^2 f^2 [\varepsilon(4\pi^2 f^2 + 1) - 1]^2}, \quad (10)$$

where f is frequency and $j = \sqrt{-1}$. This function is hump-shaped in log-log space [Fig. 2(a)], indicating that it works both as a low-pass filter and a high-pass filter. The low-pass filtering effect is due to the membrane capacitance of the model neuron, whereas the high-pass filtering effect is due to the recovery variable w . [Note that Eq. (7) without $W(s)$ indicates the low-pass filtering effect on $N(s)$.]

We assume that $\xi(t)$ has a power-law spectrum $P_N(f) = k_1 f^{-\beta}$, where k_1 is a constant. Thus, the noise variance σ_N^2 is

$$\sigma_N^2 = k_1 k_2 \int_{f_l}^{f_h} f^{-\beta} df, \quad (11)$$

where f_l and f_h , respectively, are the lower and upper limits of the noise bandwidth and k_2 is a constant. Since v can be regarded by the system as filtered $1/f^\beta$ noise, the power spectrum of the variable v [$P_v(f)$] can be expressed as

$$P_v(f) = k_1 f^{-\beta} |\chi_{v\xi}(j2\pi f)|^2. \quad (12)$$

Using Eqs. (11) and (12), the variance of v (σ_v^2) can be expressed as

$$\sigma_v^2 = h(\beta) \sigma_N^2, \quad (13)$$

where

$$h(\beta) = \frac{\int_{f_l}^{f_h} f^{-\beta} |\chi_{v\xi}(j2\pi f)|^2 df}{\int_{f_l}^{f_h} f^{-\beta} df}. \quad (14)$$

The function $h(\beta)$ represents the way in which the noise power is modulated by the system's filtering effect.

Since the $1/f^\beta$ noise used in this study is stationary, the variable v (i.e., the filtered $1/f^\beta$ noise) is also stationary with zero mean [19]. With this assumption, the (firing) frequency $\langle r_0 \rangle$ (where the brackets $\langle \rangle$ denote the ensemble average) with which the variable v crosses a threshold θ can be obtained using Rice's theorem [12,20]:

$$\langle r_0 \rangle = \left[\frac{\int_{f_l}^{f_h} f^2 P_v(f) df}{\int_{f_l}^{f_h} P_v(f) df} \right]^{1/2} \exp\left(\frac{-\theta^2}{2\sigma_v^2}\right). \quad (15)$$

By substituting Eqs. (12) and (13) into Eq. (15), we obtain

$$\langle r_0 \rangle = g(\beta) \exp\left[\frac{-\theta^2}{2h(\beta)\sigma_N^2}\right], \quad (16)$$

where

$$g(\beta) = \left[\frac{\int_{f_l}^{f_h} f^{2-\beta} |\chi_{v\xi}(j2\pi f)|^2 df}{\int_{f_l}^{f_h} f^{-\beta} |\chi_{v\xi}(j2\pi f)|^2 df} \right]^{1/2}. \quad (17)$$

If the dynamics of $S(t)$ are sufficiently slow compared to the characteristic time of the system, then the resting value of v fluctuates with time as $v(t) = S(t)/(1 + \gamma)$. Therefore, the distance to the threshold changes with time as $\theta - S(t)/(1 + \gamma)$. Taking this into account, the time-dependent firing frequency $\langle r(t) \rangle$, for $S(t)/(1 + \gamma) \ll \theta$, can be approximated as

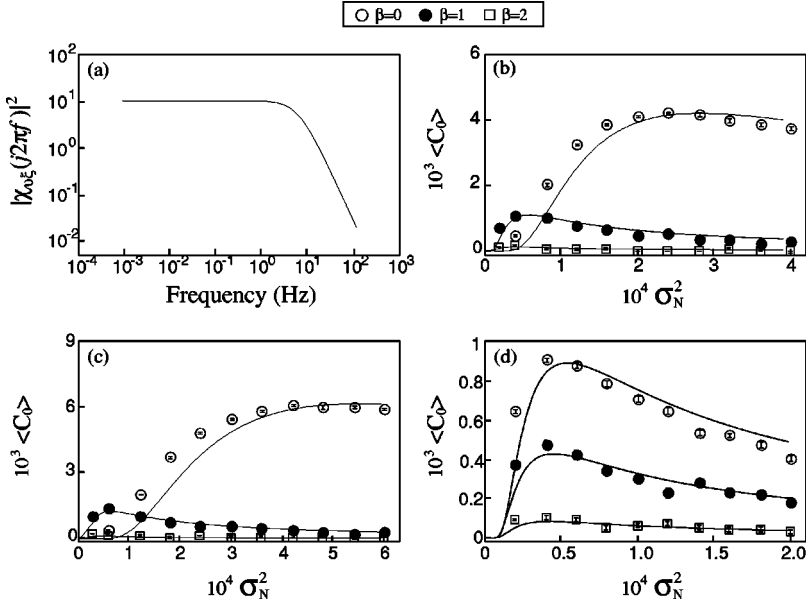


FIG. 3. (a) Squared gain of the frequency response function of the IF model given by Eq. (22). (b)–(d) Ensemble-averaged values and standard errors for C_0 (500 trials) for different levels of input noise variance σ_N^2 in the IF model (white noise, open circles; $1/f$ noise, filled circles; $1/f^2$ noise, open squares). The variance of $S(t)$ is 3.0×10^{-6} , $\gamma=0.3$, and $\theta=0.03$. The bandwidth of the noise is 0.0305–100 Hz (b), 0.0305–200 Hz (c), and 0.0305–10 Hz (d). Theoretical predictions from Eq. (20) are given by the solid lines. The amplitude of $\langle C_0 \rangle$ is adjusted for $\beta=0$. The amplitude of $\langle C_0 \rangle$ for $\beta=1$ and 2, respectively, is scaled by this value. Note that the optimal noise variance is the smallest when $\beta=2$, although this is not readily apparent for (b) and (c) because the amplitude of $\langle C_0 \rangle$ is small.

$$\langle r(t) \rangle \approx g(\beta) \exp \left[\frac{-\theta^2 + 2\theta S(t)/(1+\gamma)}{2h(\beta)\sigma_N^2} \right]. \quad (18)$$

Since the ensemble average operation does not affect $S(t)$, $\langle C_0 \rangle$ in Eq. (3) can be rewritten as

$$\langle C_0 \rangle = \langle \langle S(t) \rangle \langle R(t) \rangle \rangle. \quad (19)$$

By expanding Eq. (18) to the first order of $S(t)$ and substituting this into Eq. (19), we obtain

$$\langle C_0 \rangle \approx \frac{\theta g(\beta) \langle \langle S(t)^2 \rangle \rangle}{(1+\gamma)h(\beta)\sigma_N^2} \exp \left[-\frac{\theta^2}{2h(\beta)\sigma_N^2} \right]. \quad (20)$$

From Eq. (20), we can predict two features of the SR profile for the LFHN model: (1) the maximal value of $\langle C_0 \rangle$ is observed when $\sigma_N^2 = \theta^2/[2h(\beta)]$, and (2) the maximal value of $\langle C_0 \rangle$ is proportional to the value of $g(\beta)$. Figures 2(b)–2(d) indicate that these predictions are supported by our numerical results, i.e., the theoretical curves nicely fit the computational results.

In a previous study [13], we considered SR in a nondynamical threshold system. In that case, a narrow pulse was generated when the sum of $1/f^\beta$ noise and a given input signal crossed a threshold in a positive direction. For that system, we found that the optimal value of σ_N^2 was independent of β . In contrast, Figs. 2(b)–2(d) indicate that for the LFHN model (which includes dynamical effects), the optimal noise variance depends on the value of β . In addition, the LFHN model realizes the smallest noise variance for $1/f$ noise [Fig. 2(b)], when the noise bandwidth of Fig. 1 is used. This effect is enhanced when f_h is increased [Fig. 2(c)]; however, it is not observed when f_h is reduced [Fig. 2(d)]. Thus, the effect of minimizing the optimal noise variance with $1/f$ noise depends on the noise bandwidth.

III. INTEGRATE-AND-FIRE MODEL WITHOUT RESET

As shown in the previous section, the dynamical features of the LFHN model are essential for obtaining the described

effects of $1/f$ noise on the SR profile. One of the major characteristics of the LFHN model is the presence of a recovery variable. If the system does not have a recovery variable, then the frequency response function and the dependence of $h(\beta)$ on the value of β change. To study the effects of a recovery variable on the observed dynamics, we consider in this section the following simple model:

$$\varepsilon \dot{v} = -\gamma v + S(t) + \xi(t). \quad (21)$$

In this model, the recovery variable w of Eqs. (5) and (6) is omitted. As before, we assume that a narrow pulse is generated when v crosses a threshold value θ , without resetting. We call this model an integrate-and-fire (IF) model (without reset).

As in Sec. II, the fluctuations of v are regarded as filtered $1/f^\beta$ noise. For the IF model, the squared gain of the frequency response function for $S(t)=0$ is a well-known Lorentzian type:

$$|\chi_{v\xi}(j2\pi f)|^2 = \frac{1}{\gamma^2 + 4\pi^2 f^2 \varepsilon^2}. \quad (22)$$

This function works as a low-pass filter [Fig. 3(a)].

Figures 3(b)–3(d) show numerical results for the IF model and theoretical predictions given by Eq. (20). It can be seen that the theoretical predictions derived for the LFHN model nicely fit the computational results, i.e., they are applicable to the IF model. Although the computational results in Figs. 3(b)–3(d) look similar to those in Fig. 2(b)–2(d), an important difference should be noted: namely, that the optimal noise variance is the smallest for $\beta=2$ for all noise bandwidths. [This is ambiguous especially for (b) and (c), because the amplitude of $\langle C_0 \rangle$ is small.]

Figure 4 clearly shows that for the IF model, the optimal noise variance is the smallest for $\beta=2$. It can be seen that the value of $h(\beta)$ increases monotonically with β [Fig. 4(a)]. As pointed out in Sec. II, a larger $h(\beta)$ means that the optimal noise variance is smaller. In contrast, for the LFHN model, the value of $h(\beta)$ is maximized at intermediate val-

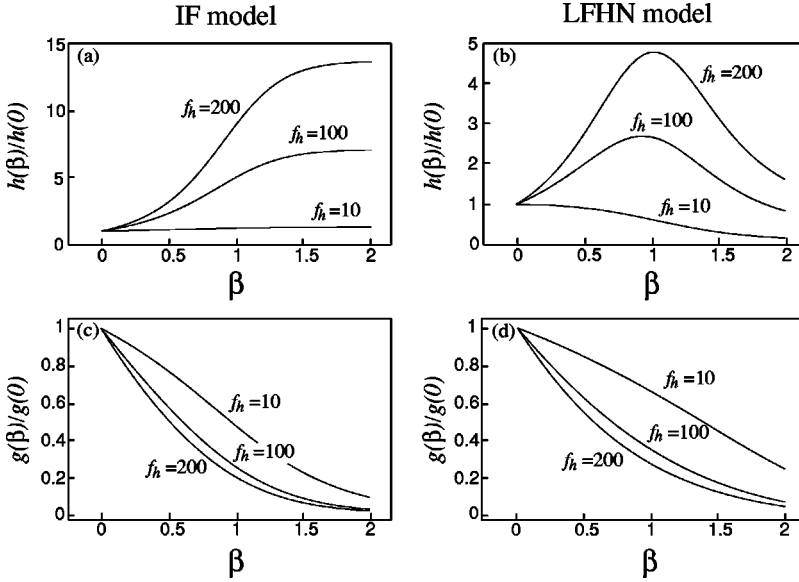


FIG. 4. Plots of $h(\beta)$ and $g(\beta)$ versus β for the IF and LFHN models. The functions $h(\beta)$ and $g(\beta)$ are calculated numerically from Eq. (14) and Eq. (17), respectively, and normalized by their respective values for $\beta=0$. The model parameters are the same as those for Fig. 2. The lower limit of the noise bandwidth f_l is fixed at 0.0305 Hz.

ues of β (between 0 and 2), except when $f_h=10$ Hz [Fig. 4(b)]. For both the IF model and the LFHN model, the value of $g(\beta)$ decreases monotonically with β [Figs. 4(c) and 4(d)].

The difference between the response of the IF model and that of the LFHN model can be explained by considering the shape of the squared gain of the frequency response function, $|\chi_{v\xi}(j2\pi f)|^2$, for the two systems. In case of the IF model, the system works as a low-pass filter to input noise [Fig. 3(a)]. The power lost by the filtering effect is the largest when $\beta=0$, because, with smaller β , a larger amount of power is distributed at higher frequencies. Considering that $h(\beta)$ represents the ratio of noise power transmitted to the filtered noise, $h(\beta)$ for the IF model increases with β monotonically. This effect does not depend on the noise bandwidth.

On the other hand, in case of the LFHN model, $|\chi_{v\xi}(j2\pi f)|^2$ is hump-shaped [Fig. 2(a)], i.e., it works not only as a low-pass filter but also as a high-pass filter. Thus, the monotonic increase of $h(\beta)$ with β cannot necessarily be expected because, while the power lost by the low-pass filtering effect decreases as β increases, the power lost by the low-pass filtering effect increases. Given that these effects are always reciprocal, $h(\beta)$ can have a maximal value at an intermediate value of β (between 0 and 2). It is important to note that the noise bandwidth can affect this relationship: for example, the high-pass filtering effect dominates when f_h is not considerably larger than f_l , which is the frequency where $|\chi_{v\xi}(j2\pi f)|^2$ is maximized [Fig. 2(a)]. Thus, $h(\beta)$ is the largest when $\beta=0$, as shown by the curve for $f_h=10$ Hz in Fig. 4(b).

Thus, a critical feature in the LFHN model for obtaining the smallest optimal noise variance with $\beta \approx 1$ is that $h(\beta)$ can be maximized when $\beta \approx 1$. In contrast, this phenomenon is never seen in the IF model, which differs from the LFHN model in that it lacks a recovery variable. We can thus conclude that a recovery variable is needed for obtaining the smallest optimal noise variance with $\beta \approx 1$.

IV. LINEARIZED FHN MODEL WITH RESET

In Sec. II, we derived a theoretical curve for $\langle C_0 \rangle$ versus σ_N^2 for the LFHN model and captured the dependence of the

optimal noise variance on the value of β . However, the LFHN model does not account for the resetting mechanism, and thus the refractory period, of the original FHN model. Therefore, in this section, we consider a more realistic model: namely, a model with the same subthreshold dynamics as the LFHN model, but one in which the values of v and w are reset to some fixed values just after a pulse is generated. (In the computer simulations, the values of v and w were reset to 1.0 and 0.15, respectively.) As a result of this resetting mechanism, a refractory period T_R (≈ 0.5 s), similar to that for the original FHN model, is realized in the model. Hereafter, we will refer to the LFHN model with reset as the RLFHN model.

Figures 5(a), 5(c), and 5(e) depict the results from computer simulations with the FHN model. The optimal noise variance is smaller for $1/f$ noise, compared to white noise, when $f_h=100$ Hz [Fig. 5(a)]; this effect is more pronounced when $f_h=200$ Hz [Fig. 5(c)]. However, this effect disappears when $f_h=10$ Hz [Fig. 5(e)]. Figures 5(b), 5(d), and 5(f) indicate that similar results can be obtained with the RLFHN model.

We now derive the theoretical prediction for $\langle C_0 \rangle$ versus σ_N^2 , using the level-crossing frequency, as in the previous sections. The basic idea is as follows: the variables v and w return, after a reset event, to the same values as those in the LFHN model because the fixed values of v and w in Eqs. (5) and (6) are stable. This means that the main difference between the RLFHN model and the LFHN model is that some action potentials are ignored in the LFHN model due to the refractory period. We consider the case where N action potentials are ignored due to the refractory period. For this case, the following inequality must hold:

$$NT < T_R < (N+1)T, \quad (23)$$

where $T=1/\langle r(t) \rangle$. Note that $\langle r(t) \rangle$ is the firing frequency for the LFHN model obtained in Sec. II. From Eq. (23), we can obtain

$$(T_R - T)/T < N < T_R/T. \quad (24)$$

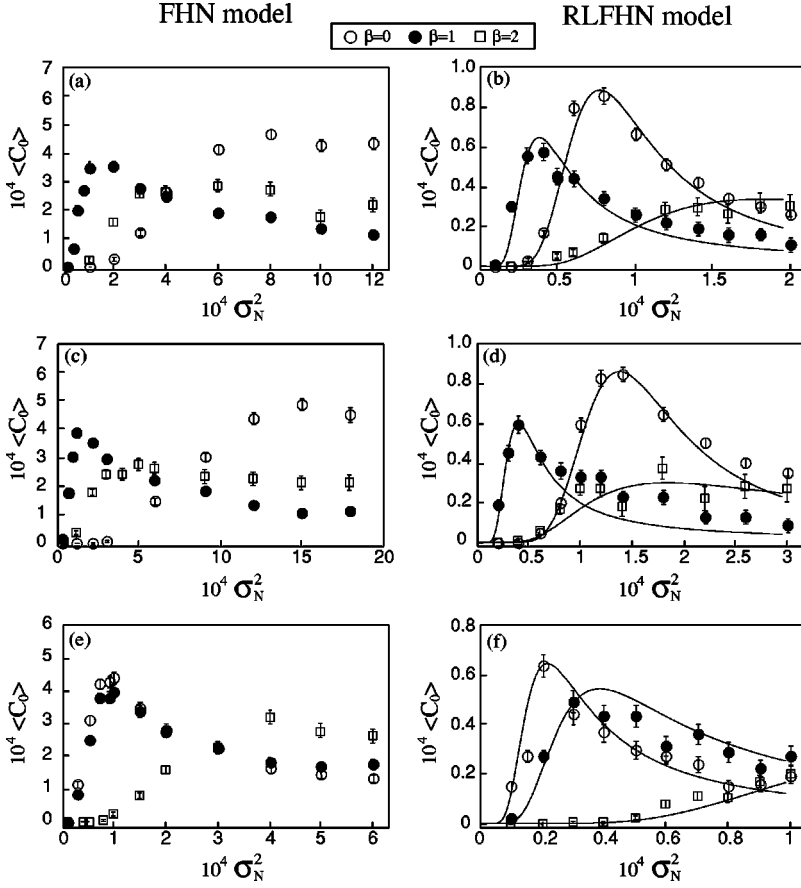


FIG. 5. Ensemble-averaged values and standard errors for C_0 (500 trials) for different levels of input noise variance σ_N^2 for the FHN model [(a), (c), and (e)] and the RLFHN model [(b), (d), and (f)]. The model parameters are the same as those for Fig. 1 (FHN model) and Fig. 2 (RLFHN model). The bandwidth of the noise is 0.0305–100 Hz [(a) and (b)], 0.0305–200 Hz [(c) and (d)], and 0.0305–10 Hz [(e) and (f)]. Theoretical predictions from Eq. (27), with $T_R=0.5$ s, are given by the solid lines. In each plot, the amplitude of $\langle C_0 \rangle$ for each type of noise is scaled by the value of $\langle C_0 \rangle$ for $\beta=0$ in the LFHN model.

We select $N=(T_R-0.5T)/T$, satisfying Eq. (24). In this case, we can expect a mean interspike interval of $(N+1)T \approx T_R+0.5T$. Therefore, the firing frequency for the RLFHN model $\langle R(t) \rangle$ is given by

$$\langle R(t) \rangle = \frac{2\langle r(t) \rangle}{1+2T_R\langle r(t) \rangle}. \quad (25)$$

Substituting Eq. (18) into Eq. (25) and expanding it in a Taylor series in $S(t)$ gives $\langle R(t) \rangle$. When $S(t)/(1+\gamma) = S_\gamma(t) \ll \theta$, retaining only the lowest-order term gives

$$\langle R(t) \rangle \approx \frac{2\langle r_0 \rangle}{1+2T_R\langle r_0 \rangle} \left[1 + \frac{\theta}{\sigma_v^2(1+2T_R\langle r_0 \rangle)} S_\gamma(t) \right]. \quad (26)$$

By substituting Eqs. (13) and (26) into Eq. (19), we obtain

$$\langle C_0 \rangle \approx \frac{2\theta\langle S(t)^2 \rangle \langle r_0 \rangle}{(1+\gamma)h(\beta)\sigma_N^2(1+2T_R\langle r_0 \rangle)^2}. \quad (27)$$

Note that Eq. (27) is also applicable to other resettable systems that have different frequency response functions.

When the results for the RLFHN model [Figs. 5(b), 5(d), and 5(f)] are compared with those for the LFHN model [Figs. 2(b), 2(c), and 2(d)], it can be seen that the optimal noise variance and the amplitude of $\langle C_0 \rangle$ for the RLFHN

model is much reduced, and the differences in amplitude of $\langle C_0 \rangle$ between the three types of noise are decreased. The theory given by Eq. (27) predicts these properties quite accurately, as shown by the solid lines in Figs. 5(b), 5(d), and 5(f).

V. INFLUENCES OF REFRACTORY PERIOD AND NOISE BANDWIDTH

In the LFHN model, the optimal noise variance and the amplitude of $\langle C_0 \rangle$ are directly related to $h(\beta)$ and $g(\beta)$, respectively [Eq. (20)]. However, in the RLFHN model, $\langle C_0 \rangle$ is dependent on various parameters, such as $h(\beta)$, $g(\beta)$, θ , and T_R , in a complex manner. Thus, analytical expressions for the maximal value of $\langle C_0 \rangle$ and the optimal noise variance cannot be obtained. Nonetheless, we can consider qualitatively how a refractory period (i.e., resetting mechanism) affects the SR profile.

To obtain the optimal noise variance, we differentiate Eq. (27) by σ_v^2 and set this to 0. The optimal value of σ_v^2 ($\sigma_{v_0}^2$) should satisfy

$$\frac{\theta^2 - 2\sigma_v^2}{\theta^2 + 2\sigma_v^2} \exp\left(\frac{\theta^2}{2\sigma_v^2}\right) = 2T_R g(\beta). \quad (28)$$

The left-hand side of Eq. (28) decreases monotonically with σ_v^2 and is equal to 0 when $\sigma_v^2 = \theta^2/2$. Therefore, $\sigma_{v_0}^2$ is less than $\theta^2/2$ because $2T_R g(\beta) > 0$. Note that $\sigma_{v_0}^2$ is equal to

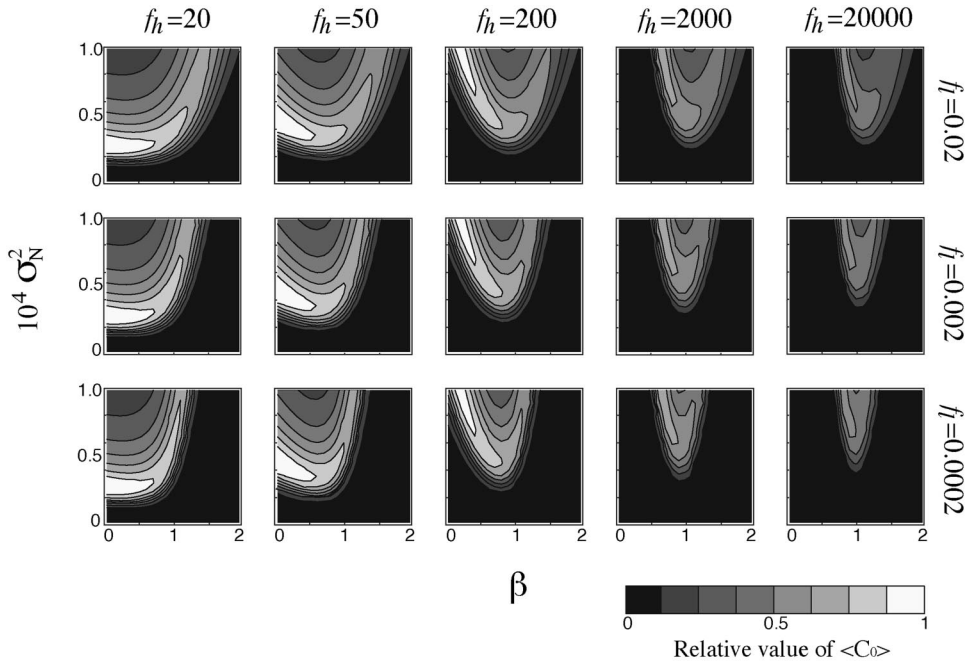


FIG. 6. Contour plots of $\langle C_0 \rangle$ versus β (abscissa) and σ_N^2 (ordinate) for various noise bandwidths in the RLFHN model. In each plot, the value of $\langle C_0 \rangle$ is normalized by the maximal value of $\langle C_0 \rangle$ for white noise ($\beta=0$). Lighter colors indicate higher values of $\langle C_0 \rangle$, as shown by the legend. These theoretical predictions are given by Eq. (27) with $T_R=0.5$. Other parameters are the same as those for Fig. 2.

$\theta^2/2$ for the LFHN model [Eq. (20)], indicating that the optimal noise variance is always smaller for the system with reset. Furthermore, assuming that $g(\beta)$ decreases monotonically with β as shown in Fig. 4(d), σ_{vo}^2 can be expected to increase with β . Thus, with a refractory period, the optimal noise variance can be minimized for $\beta \approx 1$; however, the differences between the optimal noise variance for $\beta=0$ and $\beta \approx 1$ are reduced. This can be seen by comparing results for the RLFHN model [Figs. 5(b), 5(d), and 5(f)] with those for the LFHN model [Figs. 2(b), 2(c), and 2(d)].

By substituting Eq. (28) into Eq. (27), the maximal value of the cross power, $\langle C_0 \rangle_{\max}$, can be obtained as

$$\langle C_0 \rangle_{\max} \propto \Delta g(\beta), \quad (29)$$

where

$$\Delta = \frac{(\theta^2 + 2\sigma_{vo}^2)^2}{\sigma_{vo}^2} \exp\left(-\frac{\theta^2}{2\sigma_{vo}^2}\right). \quad (30)$$

Equation (29) indicates that $\langle C_0 \rangle_{\max}$ in the LFHN model [$\propto g(\beta)$] is modulated by Δ , which is a monotonically increasing function of σ_{vo}^2 . Considering that σ_{vo}^2 increases with β while $g(\beta)$ decreases with β , Δ is also a monotonically increasing function of β . Thus, the refractory period in the RLFHN model works to reduce the differences in the value of $\langle C_0 \rangle_{\max}$ for different β , as can be seen by comparing results for the RLFHN model [Figs. 5(b), 5(d), and 5(f)] with those for the LFHN model [Figs. 2(b), 2(c), and 2(d)].

The SR profile is also affected by the noise bandwidth via both $g(\beta)$ and $h(\beta)$. More specifically, the effect of minimizing the optimal noise variance with $1/f$ noise depends on the noise bandwidth, as shown in Fig. 5. Figure 6 depicts contour plots of the theoretical predictions for $\langle C_0 \rangle$ versus β and σ_N^2 for various noise bandwidths in the RLFHN model [Eq. (27)]. When $f_h=20$ Hz, the ability to detect a sub-threshold signal, from the standpoint of minimizing the optimal noise variance and maximizing $\langle C_0 \rangle_{\max}$, is the greatest

for $\beta \approx 0$. However, as f_h increases, the superiority of $\beta \approx 1$, in terms of minimizing the optimal noise variance, becomes clearer (Fig. 6). On the other hand, the value of $\langle C_0 \rangle_{\max}$ for $\beta \approx 1$ relative to that for $\beta=0$ decreases as f_h increases. It is interesting to note, however, that the value of $\langle C_0 \rangle_{\max}$ of the RLFHN model for $\beta \approx 1$ is maintained to be approximately 50% of that for $\beta=0$ even when f_h reaches 20 000 Hz. This relatively high level of $\langle C_0 \rangle_{\max}$ for $\beta \approx 1$ is due to the refractory period, because in the LFHN model, which lacks a refractory period, the value of $\langle C_0 \rangle_{\max}$ for $\beta \approx 1$ is suppressed to approximately 4% of that for $\beta=0$ when f_h reaches 20 000 Hz. The value of f_l does not have a significant influence on these effects. As discussed in Sec. III, if f_l is larger than f_t or if f_h is smaller than f_t , then the superiority of $1/f$ noise cannot be expected.

VI. CONCLUSIONS AND IMPLICATIONS

Here we showed that in a linearized version of the FHN model, the optimal noise variance for SR can be minimized when $1/f^\beta$ noise with $\beta \approx 1$ is added to the system. As we noted, similar dynamics are exhibited by the original FHN model. We also showed that the linearized model allows one to obtain the theoretical curve for $\langle C_0 \rangle$ versus σ_N^2 and to clarify the mechanisms underlying this phenomenon. Specifically, we showed that when $\beta \approx 1$, the interaction of the low-pass filtering effect of the membrane capacitance of the model neuron and the high-pass filtering effect of the recovery variable serves (1) to shape the squared gain of the frequency response function in the form of a hump, and (2) to maximize the power transfer ratio from the input noise to the membrane voltage. Moreover, we showed that in terms of the input-output coherency, the existence of a refractory period is advantageous for $\beta \approx 1$.

The aforementioned dynamical properties are found in real neurons. Thus, if the noise bandwidth satisfies certain conditions, $1/f$ noise may be better than white noise for producing SR in real neural systems. The same effect, using the

output signal-to-noise ratio as the input-output coherence measure, has been demonstrated theoretically in model neurons and experimentally in rat sensory neurons [21].

Although $1/f$ noise is commonly observed in physiological systems [7–10], its functional significance has not been fully elucidated. Our finding that $1/f$ noise can be suitable for SR in model neurons leads to the hypothesis that $1/f$ noise might be operative in certain neural systems for detecting weak signals.

ACKNOWLEDGMENTS

The authors thank D. Mar for useful discussions. This work was supported by the Japan Society for the Promotion of Science for Young Scientists (D.N.), the U.S. National Science Foundation (J.J.C.), the U.S. Department of Energy (J.J.C.), the Japanese Ministry of Education, Science and Culture (Y.Y.), the Japan Space Foundation (Y.Y.), and the Japanese Science and Technology Agency (Y.Y.).

-
- [1] F. Moss, D. Pierson, and D. O’Gorman, *Int. J. Bifurcation Chaos Appl. Sci. Eng.* **4**, 1383 (1994); K. Wiesenfeld and F. Moss, *Nature (London)* **373**, 33 (1995); A. R. Bulsara and L. Gammaitoni, *Phys. Today* **49**(3), 39 (1996); L. Gammaitoni, P. Hänggi, P. Jung, and F. Marchesoni, *Rev. Mod. Phys.* **70**, 223 (1998).
- [2] R. Benzi, A. Sutera, and A. Vulpiani, *J. Phys. A* **14**, L453 (1981); C. Nicolis, *Tellus* **34**, 1 (1982); R. Benzi, G. Parisi, A. Sutera, and A. Vulpiani, *ibid.* **34**, 10 (1982); S. Fauve and H. Heslot, *Phys. Lett.* **97A**, 5 (1983).
- [3] B. McNamara, K. Wiesenfeld, and R. Roy, *Phys. Rev. Lett.* **60**, 2626 (1988); B. McNamara and K. Wiesenfeld, *Phys. Rev. A* **39**, 4854 (1989).
- [4] A. Longtin, A. Bulsara, and F. Moss, *Phys. Rev. Lett.* **67**, 656 (1991); A. Longtin, *J. Stat. Phys.* **70**, 309 (1993); F. Moss *et al.*, *Ann. N.Y. Acad. Sci.* **706**, 26 (1993); K. Wiesenfeld *et al.*, *Phys. Rev. Lett.* **72**, 2125 (1994).
- [5] J. J. Collins, C. C. Chow, and T. T. Imhoff, *Phys. Rev. E* **52**, R3321 (1995); *Nature (London)* **376**, 236 (1995); J. J. Collins, C. C. Chow, A. C. Capela, and T. T. Imhoff, *Phys. Rev. E* **54**, 5575 (1996).
- [6] J. K. Douglass, L. Wilkens, E. Pantazelou, and F. Moss, *Nature (London)* **365**, 337 (1993); J. E. Levin and J. P. Miller, *ibid.* **380**, 165 (1996); P. Cordo *et al.*, *ibid.* **383**, 769 (1996); J. J. Collins, T. T. Imhoff, and P. Grigg, *ibid.* **383**, 770 (1996); J. J. Collins, T. T. Imhoff, and P. Grigg, *J. Neurophysiol.* **76**, 642 (1996); R. P. Morse and E. F. Evans, *Nature Med.* **2**, 928 (1996); B. J. Gluckman *et al.*, *Phys. Rev. Lett.* **77**, 4098 (1996); J. J. Collins, T. T. Imhoff, and P. Grigg, *Phys. Rev. E* **56**, 923 (1997); K. A. Richardson *et al.*, *Chaos* **8**, 599 (1998).
- [7] A. L. Goldberger, D. R. Rigney, and B. J. West, *Sci. Am.* **262**, 34 (1990); J. B. Bassingthwaighe, L. S. Lievovitch, and B. J. West, *Fractal Physiology* (Oxford University Press, New York, 1994).
- [8] M. C. Teich, *IEEE Trans. Biomed. Eng.* **36**, 150 (1989).
- [9] Y. Yamamoto and R. L. Hughson, *Physica D* **68**, 250 (1993); *Am. J. Physiol.* **266**, R40 (1994); Y. Yamamoto, J.-O. Fortrat, and R. L. Hughson, *ibid.* **269**, H480 (1995); Y. Yamamoto *et al.*, *ibid.* **269**, R830 (1995).
- [10] J. J. Collins and C. J. DeLuca, *Exp. Brain Res.* **95**, 308 (1993); *Phys. Rev. Lett.* **73**, 764 (1994); J. M. Hausdorff *et al.*, *J. Appl. Physiol.* **78**, 349 (1995); D. Nozaki, K. Nakazawa, and Y. Yamamoto, *Exp. Brain Res.* **105**, 402 (1995); **112**, 112 (1996); Y. Chen, M. Ding, and J. A. Kelso, *Phys. Rev. Lett.* **79**, 4501 (1997).
- [11] L. B. Kiss *et al.*, *J. Stat. Phys.* **70**, 451 (1993).
- [12] Z. Gingl, L. B. Kiss, and F. Moss, *Europhys. Lett.* **29**, 191 (1995).
- [13] D. Nozaki and Y. Yamamoto, *Phys. Lett. A* **243**, 281 (1998).
- [14] R. A. FitzHugh, *Biophys. J.* **1**, 445 (1961); J. Nagumo, S. Arimoto, and S. Yoshizawa, *Proc. IRE* **50**, 2061 (1962).
- [15] In this study, we used Gaussian $1/f^\beta$ noise ($0 \leq \beta \leq 2$) with zero mean and upper and lower limits on the frequency range. The $1/f^\beta$ noise was generated by the spectrum-based method described in Ref. [13].
- [16] We used the fourth-order Runge-Kutta method for digital simulation (time step of 0.002 s; total time, 32.768 s). The impulse trains were convolved by a symmetric Hanning window (width = 6 s) to estimate $\langle R(t) \rangle$, where the brackets $\langle \rangle$ denote the ensemble average. The signal $S(t)$ was formed by convolving Gaussian white noise with the same window function.
- [17] H. A. Kramers, *Physica* **7**, 284 (1940).
- [18] P. Hänggi, P. Jung, C. Zerbe, and F. Moss, *J. Stat. Phys.* **70**, 25 (1993).
- [19] A. Papoulis, *Probability, Random Variables, and Stochastic Processes*, 3rd ed. (McGraw-Hill, New York, 1991).
- [20] S. O. Rice, in *Selected Papers on Noise and Stochastic Processes*, edited by N. Wax (Dover, New York, 1954).
- [21] D. Nozaki, D. J. Mar, P. Grigg, and J. J. Collins, *Phys. Rev. Lett.* **82**, 2402 (1999).